

Invariant Image Reparameterisation: A Unified Approach to Structural and Practical Identifiability and Model Reduction

Oliver J. Maclaren*, Ruanui Nicholson*, Joel A. Trent*, Joshua Rottenberry[†], and Matthew J. Simpson[‡]

Abstract. Both structural and practical parameter non-identifiability present fundamental challenges when using mathematical models to interpret data. This issue is particularly acute in complex, applied areas such as the life sciences or engineering, where determining appropriate model complexity is challenging. While several approaches exist for diagnosing and resolving parameter non-identifiability, including symbolic methods, profile likelihood analysis, and sloppiness analysis, these approaches have distinct limitations and are rarely combined. We present an integrated approach called Invariant Image Reparameterisation (IIR) that incorporates key elements of these methods in a new way. Our approach replaces symbolic computations with numerical calculations at a single reference estimate and an invariance condition that determines when this local calculation holds globally. Parameter combinations determined by this method are naturally ordered by degree of identifiability, and this supports model reduction by replacing a practically non-identified model with a structurally non-identified approximate model. This approximate model can be further parameterised in terms of identified parameters only. By treating parameter combinations determined by our approach as interest parameters within our established likelihood-based Profile-Wise Analysis (PWA) framework, we incorporate uncertainty quantification in terms of likelihood profiles and confidence sets. We provide a Julia library on [GitHub](#) demonstrating our methodology across a range of mathematical models.

Key words. Identifiability, Parameter estimation, Model reduction, Uncertainty quantification, Prediction

1. Introduction. Mechanistic mathematical models are widely used for interpreting experimental and observational data and learning about underlying causes of the observed phenomena. Such models are routinely used to provide insight into a broad range of applications including engineering (e.g. material science [38], fluid dynamics and transport phenomena [4, 30, 64, 6, 41]), ecology and population biology [40], disease transmission dynamics [58] as well as chemical reactions [37] and econometrics [34]. A fundamental challenge is determining whether available data contain enough information to yield unique or sufficiently precise parameter estimates, which are crucial both for understanding mechanisms and making predictions [66, 67].

Establishing whether model parameters are uniquely determined by ideal or ‘infinite’ data is often referred to as *structural identifiability analysis* in the modelling literature [5, 17, 47, 52, 53, 26], and is also simply referred to as identifiability analysis in the statistical literature [48]. In contrast, learning whether sufficiently precise parameter estimates are possible when working with finite noisy observations corresponds to the notion of *practical identifiability* (or estimability) analysis [35, 48, 72, 43].

Parameter non-identifiability occurs when different combinations of parameters produce

*Department of Engineering Science and Biomedical Engineering, University of Auckland, Auckland 1142, New Zealand (oliver.maclaren@auckland.ac.nz).

[†]School of Mathematical Sciences, Queensland University of Technology (QUT), Brisbane, Australia.

[‡]ARC Centre of Excellence for the Mathematical Analysis of Cellular Systems, QUT, Brisbane, Australia.

identical, or sufficiently close, model outputs, making it impossible to uniquely determine the underlying mechanisms from even perfect observations of the outputs [48, 67].

When model parameters are not identifiable, key questions arise: Can we identify certain parameter combinations even when individual parameters are non-identifiable [48, 18]? Can we perform model reduction to obtain simpler, identifiable models [14, 15, 29, 52, 53, 18]? Can we use practical non-identifiability to guide experimental design [65] or motivate approximate model reduction [51]? Various approaches to addressing such questions include symbolic methods [14, 15, 19, 16], profile likelihood analysis [42, 62, 51, 66, 70], and sloppiness analysis [9, 33, 55]. Related work in large-scale inverse problems includes active subspaces [20, 7] and likelihood-informed dimension reduction [24, 25]. While each approach has strengths, they also have limitations: symbolic methods typically apply only to idealised data/structural identifiability scenarios, profile likelihood methods usually require user choice of target parameter to analyse, and sloppiness analysis may use non-parameterisation-invariant approximations for uncertainty quantification.

While systematic approaches to parameter subset selection for profile likelihood analysis have been developed, e.g. using Fisher Information Matrix analysis combined with profile likelihood [27] or context-dependent analysis along profiles [51], these approaches still require careful parameter subset selection steps and determination of functional relationships from profiles. The connection between sloppiness and identifiability is also somewhat unclear, as sloppiness is a relative notion quantified in terms of ratios of eigenvalues (or singular values) and models can be sloppy yet identifiable [17]. In applications of sloppiness and profile likelihood analysis to model reduction, users often simply set poorly-identified parameters to zero or some arbitrary value [44, 28, 71]. However, this can lead to setting individually poorly-identified parameters to values that jointly violate the requirements on possible values for the well-identified parameter combinations. Model reduction methods for inverse problems [20, 24], while powerful for computation, particularly Bayesian inverse problems, do not typically directly address identifiability questions (though see [7]) and do not usually aim to provide interpretable parameter combinations for mechanistic models.

We present a novel approach that: (i) automatically identifies well-identified parameter combinations without symbolic computation; (ii) enables model reduction without requiring an explicit reduced form model; and (iii) provides statistically sound interval estimates for both parameters and predictions. Our method combines ideas from symbolic analysis and sloppiness literature to convert the general symbolic problem to a numerical one solvable at a single reference point. These parameter combinations then serve as interest parameters in our Profile-Wise Analysis (PWA) framework [67, 66]. For models expressible as functions of monomial parameter combinations, we recover structural identifiability analysis results to arbitrary accuracy, while still discovering useful approximate monomial combinations in other cases. Our approach also allows for non-integer powers in the ‘monomial’ combinations.

To illustrate these ideas, we first apply our method to a simple statistical model with practical identifiability issues and an approximate limiting model, before considering mechanistic models based on differential equations.

2. Methods. Here, we outline the technical foundations of our ‘Invariant Image Reparameterisation’ approach, which builds on and extends the frameworks reviewed in [19], [18],

[66], and, indirectly, [48, 49]. Our approach consists of four key components: (1) an auxiliary mapping connecting model parameters to observable quantities, (2) a general reparameterisation framework, (3) an initial parameter transformation to enable numerical computation, and (4) a singular value decomposition for implementing the reparameterisation in transformed parameter space. The identified parameter combinations can then serve as interest parameters in our Profile-Wise Analysis (PWA) workflow [66] or alternative approaches like Bayesian inference, which can also benefit from reparameterisation methods [31].

2.1. Terminology. We work relatively informally with (assumed-to-be) smooth mappings between finite-dimensional spaces [46], using standard terminology for submersions – mappings with full rank derivative – and immersions – mappings with injective derivative. The observed Fisher information measures local parameter information content via the negative Hessian of the log-likelihood [60, 21, 61], with zero eigenvalues indicating parameter redundancy and potential non-identifiability [13]. While we mention the Fisher information as a complementary approach to detecting parameter redundancy, our primary focus is on working directly with the auxiliary mapping and likelihood. Informally, parameters or parameter combinations are identifiable if they can be uniquely determined from ‘perfect data’. In the context of a model mapping parameters to data distributions, $\theta \mapsto p(y; \theta)$, this is equivalent to the mapping, or more generally an induced relation in terms of parameter combinations, being injective [48].

2.2. Model representation. The auxiliary mapping ϕ connects model parameters to data distribution parameters [66]:

$$(2.1) \quad \theta \mapsto \phi(\theta),$$

with density function

$$(2.2) \quad p(y; \phi),$$

inducing the probability model

$$(2.3) \quad p(y; \theta) = p(y; \phi(\theta)).$$

For spatial/temporal models, we use numerical solutions on a fine grid as the ‘exhaustive’ summary, evaluating derivatives via automatic differentiation in Julia [63]. Thus, while our approach is essentially identical to the ‘exhaustive summary’ approach reviewed by [19, 18], we generally avoid the need for explicit exhaustive summary methods such as Taylor series or generating series (as reviewed in the cited articles), though these can be used if available. In this context, we emphasise that automatic differentiation at the source code level is distinct from symbolic differentiation and only evaluates the numerical value of the derivative at a fixed input value [32]. Numerical solutions are typically more readily available and applicable than symbolic methods for complex models.

The observed Fisher information in θ coordinates is:

$$(2.4) \quad \mathcal{J}(\theta) = -H_l(\theta; y) = -\nabla_{\theta}(D_{\theta}l(\theta; y))^T = -\frac{\partial^2 l(\theta; y)}{\partial \theta \partial \theta^T}$$

where $l(\theta; y)$ is the log-likelihood, $D_{\theta}f$ is the Jacobian, $\nabla_{\theta}f$ is the gradient, and H_f is the Hessian [50].

2.3. Decomposition of the auxiliary mapping. The auxiliary mapping can be decomposed as:

$$(2.5) \quad \phi(\theta) = \tilde{\phi}(\psi(\theta)),$$

where $\psi(\theta)$ represents identifiable parameter combinations and $\tilde{\phi}$ provides a one-to-one mapping to data distribution parameters. This decomposition is guaranteed by the epi-mono factorisation property of the general category of sets and mappings [45], where any mapping $f : A \rightarrow B$ between sets A and B factorises as the composition:

$$(2.6) \quad f = m \circ e,$$

where $e : A \rightarrow C$ is onto (epimorphic), $m : C \rightarrow B$ is one-to-one (monomorphic), and C is some intermediate space, called the *image*, $\text{im}(f)$, in the context of category theory. Conceptually, this represents the possibility of a reduced model taking just the identified parameter combinations. Here we aim to determine this intermediate image by a local calculation that is ‘invariant’ to the choice of calculation point.

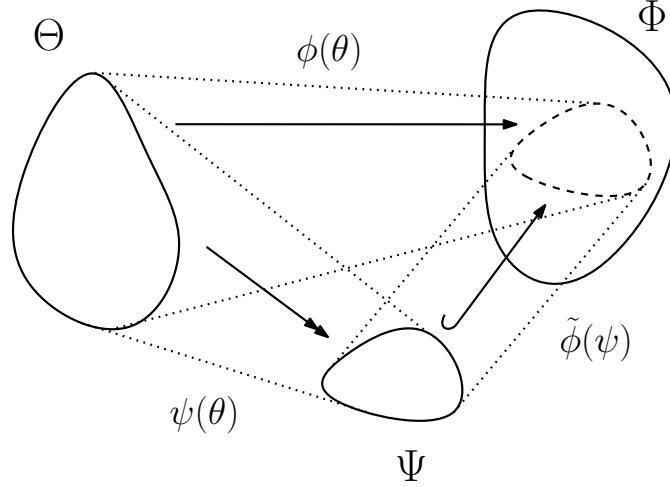


Figure 1: The basic decomposition of the auxiliary mapping into an identifiable reparameterisation followed by a reduced model mapping. Here θ represent the original model parameters, $\psi(\theta)$ represents identifiable parameter combinations, and $\tilde{\phi}$ provides a one-to-one mapping from identifiable parameter combinations to data distribution parameters.

2.4. Symbolic reparameterisation condition. For smooth mappings with constant rank, we can strengthen the epi-mono factorisation by requiring $\psi(\theta)$ to be a smooth submersion and $\tilde{\phi}(\psi)$ to be a smooth immersion [46]. The chain rule then gives:

$$(2.7) \quad D_{\theta}\phi(\theta) = D_{\psi}\tilde{\phi}(\psi(\theta))D_{\theta}\psi(\theta).$$

Since $D_\psi \tilde{\phi}(\psi(\theta))$ is one-to-one, the rank of $D_\psi \tilde{\phi}(\psi(\theta))$ and $D_\theta \phi(\theta)$ are the same; furthermore, these derivatives share the same null space/kernel (see supplementary material):

$$(2.8) \quad \ker D_\theta \psi(\theta) = \ker D_\theta \phi(\theta).$$

Given null space vectors $\alpha(\theta)$ obtained from $D_\theta \phi(\theta)$, we can then solve the differential condition:

$$(2.9) \quad D_\theta \psi(\theta) \alpha(\theta) = 0,$$

for $\psi(\theta)$. This is equivalent to the conditions given by e.g. [13, 14], summarised by [19, 18]. It is also equivalent to equating the rows of $D_\theta \psi(\theta)$ to the vectors spanning the row space of $D_\theta \phi(\theta)$, which gives a system of differential equations for ψ . The image of the parameter space Θ under the resulting ψ gives the intermediate ‘image’ component C of the epi-mono factorisation. A concrete example of solving the above symbolic condition is provided in the Results section.

As shown in the supplementary material, we can also work directly with the observed Fisher information by solving a null space constraint in terms of the Fisher information rather than the Jacobian derivative of the auxiliary mapping. For spatial or temporal models, we need to account for the functional nature of the model outputs. While we adopt a discretisation approach to representing model outputs, here the discretisation level used – solution grid or observation grid – matters. In particular, the auxiliary mapping and the observed Fisher information must be defined on the same grid level for the null spaces to match, otherwise additional null space components may be introduced (see supplementary material and discussion below). As we work with the auxiliary mapping defined on the solution grid level for determining the reparameterisation, this is only relevant for potential comparisons to Fisher information-based methods.

2.5. Parameter space linearisation. Our goal is to determine identifiable parameter combinations without symbolic computation. While numerical methods typically provide only local reparameterisation information, we show that an initial coordinate transformation enables global results. Here we focus on the componentwise log transformation $\log \theta = [\log \theta_1, \log \theta_2, \dots, \log \theta_p]^T$, which linearises monomial parameter combinations in parameter space, though the overall function will still typically be a nonlinear function of the resulting linear combinations of log parameters. Reduced sets of monomial parameter combinations commonly arise in mechanistic models, e.g. via the Buckingham Pi theorem of dimensional analysis [11], and related asymptotic approximations and model reduction [3]. Such a log parameter transformation is commonly used in the sloppiness literature [8, 56, 71] and this also inspired our present approach. However, our basic approach can be applied if, e.g., only some components are logged or even if both logged and unlogged parameters are considered simultaneously.

To work in log coordinates, we define $\theta^* = \log(\theta)$ to be the componentwise log of the parameter vector, and define $\phi_*(\theta^*) = \phi(\theta)$ and $\psi_*(\theta^*) = \psi(\theta)$ to be the corresponding mappings in log coordinates. Models that can be written in terms of monomial parameter combinations take the form:

$$(2.10) \quad \phi(\theta) = \phi_*(\theta^*) = \tilde{\phi}(\exp(A\theta^*)),$$

where A is a matrix of coefficients and $\tilde{\phi}$ is the intermediate mapping in (2.5). The chain rule gives:

$$(2.11) \quad D_{\theta^*} \phi_*(\theta^*) = D_{\psi_*} \tilde{\phi}(\psi_*(\theta^*)) \text{diag}(\exp(A\theta^*))A,$$

leading to our key condition:

$$(2.12) \quad \ker A = \ker D_{\theta^*} \phi_*(\theta^*).$$

This follows since the first term on the right-hand side of the chain rule equation (2.11) is injective by assumption, and the second term is a diagonal matrix of exponential entries (which are hence non-zero) and is therefore injective. As before (see also supplementary material), these leave the null space of A unchanged. As the left-hand side of (2.12) is parameter-independent, the right-hand side must be too. We can hence evaluate the right-hand side derivative at any convenient point to determine the global, invariant null space, complementary row space and hence intermediate image, reducing what would be a PDE to an algebraic computation. If the model is assumed non-identifiable, the point used will generally be, e.g., any (non-unique) maximum likelihood estimate, and the Jacobian will be singular. This is expected and causes no issues in general.

While the above condition does not uniquely determine A , as any basis for the null space (and complementary row space) can be used, it establishes the existence of a matrix capturing non-identifiable and identifiable parameter combinations. While the coefficients in A are traditionally restricted to integers in dimensional analysis, here we allow them to be arbitrary real numbers and do not require the combinations to be dimensionless *a priori*. This relaxation facilitates numerical computation and provides more flexibility in discovering practically useful parameter combinations. However, we also consider *a posteriori* scaling and rounding operations to convert these real-valued coefficients to integers to aid interpretability while preserving key properties of the approximation.

The corresponding alternative route to the decomposition of the auxiliary mapping is illustrated in Figure 2.

2.6. Singular value decomposition for nonlinear parameter combinations. Given the Jacobian in log-parameters at reference point $\hat{\theta}^*$, we compute:

$$(2.13) \quad D_{\theta^*} \phi_*(\hat{\theta}^*) = U\Sigma V^T = U_r \Sigma_r V_r^T.$$

Taking $A = V_r^T$, or any row-scaled version of this, ensures the same kernel as $D_{\theta^*} \phi_*(\hat{\theta}^*)$. The singular values provide a natural ranking of parameter combinations by identifiability. Zero or near-zero values indicate structural or practical non-identifiability, respectively, corresponding to insensitivity of the auxiliary mapping to these parameter combinations. The associated singular vectors provide the associated parameter combinations. The SVD is chosen because it is generally numerically stable and provides an orthogonal basis for the parameter space, maximising the separation of information concerning the different parameter combinations (see also [2, 22]).

We can also partition parameters into identifiable and non-identifiable combinations using the full, rather than reduced, SVD:

$$(2.14) \quad \theta \mapsto \begin{bmatrix} \psi(\theta) \\ \lambda(\theta) \end{bmatrix} = \exp(V^T \log(\theta)),$$

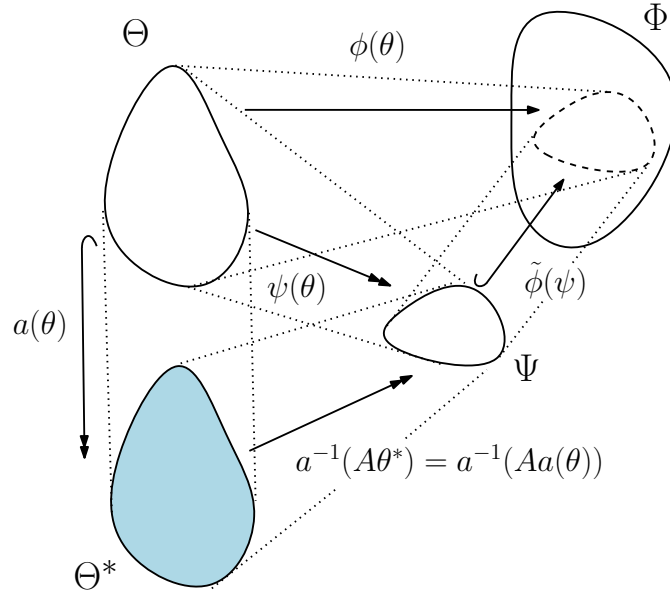


Figure 2: Implementation of parameter space linearisation using an initial componentwise transformation $a(\theta)$, typically log, followed by a linear transformation and componentwise inverse. The chain rule applied on the path from Θ^* to Φ allows us to equate the overall null space to that of the constant linear transformation A .

where $\psi(\theta)$ corresponds to non-zero singular values and associated singular vectors, and $\lambda(\theta)$ to (near) zero values and associated singular vectors. This maintains compatibility with existing model codes that require full parameter vectors, while capturing the identifiability structure.

In the case of practical non-identifiability, or near non-identifiability, there will be singular values close to zero, and the corresponding singular vectors will be elements of the row space rather than the null space of the Jacobian. As the SVD leads to an orthogonal basis these singular vectors can still be considered to span a self-contained ‘practically non-identifiable’ parameter space (see e.g. [68]), and the remaining singular vectors will still span the well-identified parameter space.

2.7. Practical vs structural identifiability and observation operators. An important aspect of the relationship between practical and structural identifiability for spatial or temporal models is represented by the need for observation operators, such as:

$$(2.15) \quad \phi_{\text{obs}} = B_{\text{obs}}\phi_{\text{fine}}$$

where B_{obs} maps the fine-scale (numerical) solution to (experimental) observation points. The additional loss of information due to coarser observation scale can introduce additional null space components or poorly-identified parameters depending on the degree of additional discretisation (see supplementary material).

When analysing at the solution grid level, our results should, to numerical approximation, recover those from an idealised structural identifiability analysis. However, for ill-posed problems or models with parameter-dependent limiting behavior, the distinction between practical and structural non-identifiability can blur [48]. The auxiliary mapping may have arbitrarily small singular values in certain parameter regions, making the distinction between practical and structural non-identifiability less clear. Furthermore, it is unclear if ideal structural identifiability results are useful in the absence of practical identifiability [48]. Our approach here is to use the auxiliary mapping at the solution grid level to determine the reparameterisation based on the full SVD in log coordinates. This reparameterisation allows us to group parameters according to degree of identifiability rather than strict identifiability or non-identifiability, making the distinction between practical and structural identifiability is less critical for our approach. However, given a parameterisation, we carry out the likelihood-based uncertainty analysis at the observation grid level to further reflect the practical identifiability of the model. Thus we provide a practical identifiability analysis that is consistent with, but not reliant on, idealised structural identifiability analysis.

2.8. Scaling and rounding. For numerical implementation, we apply scaling and rounding to singular vectors to obtain interpretable parameter combinations, defaulting to the nearest 0.5 when scaling relative to the smallest non-zero singular value. The continuity of singular subspaces [68] ensures stable separation of parameter combinations in cases of near non-identifiability, with practically (non-)identifiable subspaces corresponding to structurally (non-)identifiable subspaces of the limit model.

2.9. Profile-wise analysis. We quantify uncertainty using our PWA framework [66], which connects identifiability, parameter estimation, and predictive uncertainty through likelihood-based confidence sets. This approach uses both the joint likelihood for all parameters and profile likelihoods, where the likelihood is evaluated as a function of a target parameter while maximising over the other ‘nuisance’ parameters for each value of the target parameter [42, 62, 21, 61]. We implement our methods numerically in Julia, with full details, including the packages used, available in the [repository](#).

As the likelihood function is invariant to reparameterisation [60, 61, 21], reparameterisation of the full likelihood preserves all information in the original likelihood, unlike quadratic approximations based on the Fisher information. Rather, reparameterisation presents the information in the likelihood in a clearer form, while profile likelihoods reveal identifiability of individual parameters, or parameter combinations, separately from nuisance parameters [2].

3. Example models. Here, we describe three examples of varying areas of application and complexity, covering statistics and data science (parameterised normal distributions based on approximations to the binomial and Poisson models) [59, 2, 1], biochemistry and bioengineering (Michaelis-Menten kinetics) [54, 39], and physics and engineering (groundwater flow, heat conduction, diffusive and other transport modelling) [4, 30, 64, 12, 23, 6].

3.1. Parameterised normal approximations. Our first example considers estimating the number of trials n and success probability p in a continuous approximation to a binomial model. Near the Poisson limit (large n , small p), maximum likelihood estimates become unstable [59], providing a case study in practical non-identifiability.

The model for a single (n -trial) experiment is:

$$(3.1) \quad Y \sim \mathcal{N}(np, np(1 - np)),$$

with Poisson limit case:

$$(3.2) \quad Y \sim \mathcal{N}(np, np).$$

The auxiliary mapping connects the underlying (n, p) ‘mechanistic’ parameters to normal distribution parameters:

$$(3.3) \quad \phi : \begin{bmatrix} n \\ p \end{bmatrix} \mapsto \begin{bmatrix} np \\ np(1 - p) \end{bmatrix} = \begin{bmatrix} \mu \\ \sigma^2 \end{bmatrix}.$$

Although this is not really a ‘mechanistic’ model in the usual sense, one could consider an underlying binomial model is a lower-level mechanism that ‘generates’ the higher-level (approximately) normally distributed observations. The problem is to determine both n and p given k observations from the single experiment model given by (3.1) or (3.2).

3.2. Michaelis-Menten kinetics. Our second example is the Michaelis-Menten model [39, 54]. This equation describes substrate depletion:

$$(3.4) \quad \frac{dS}{dt} = -\frac{\nu S}{K + S},$$

where S is substrate concentration, ν is maximum growth rate, and K is the half-saturation constant. For low substrate concentrations relative to K , this model has practical identifiability issues (see [36] in the context of microbial growth models), and the model approximately reduces to:

$$(3.5) \quad \frac{dS}{dt} = -\frac{\nu}{K} S.$$

The auxiliary mapping takes parameter vector $\theta = [\nu, K]^T$ to a vector of solution values $s(\theta)$ defined on a fine time grid. For simplicity, we assume a normal distribution error model with constant standard deviation $\sigma = 0.05$, though, e.g., log-normal errors or other error models can also be considered easily within our framework [57] (see also the next example). Observations then follow:

$$(3.6) \quad s_{\text{obs}} \sim \mathcal{N}(B_{\text{obs}}s(\theta), \sigma^2 I),$$

where B_{obs} maps to observation points and $\sigma = 0.05$.

In our present work we use the (structural) auxiliary mapping to determine the reparameterisation, but the point estimate is determined by using the likelihood based on the observed data distribution above.

3.3. Flow in heterogeneous media. Our final example models groundwater flow in a heterogeneous aquifer [4, 30, 64], governed by:

$$(3.7) \quad T_i \frac{d^2 h}{dx^2} + R = 0,$$

for regions $i = 1, 2$, with transmissivity T_i and recharge rate R . Boundary conditions enforce zero head at endpoints and continuity at the interface:

$$(3.8) \quad \begin{aligned} h_1(0) &= 0 \\ h_2(L) &= 0 \\ h_1(L/2) &= h_2(L/2) \\ -T_1 \frac{dh_1}{dx}(L/2) &= -T_2 \frac{dh_2}{dx}(L/2). \end{aligned}$$

Analogous models appear in heat conduction, diffusive transport, and other transport phenomena [12, 23, 6].

The solution (supplementary information) depends only on ratios R/T_1 and R/T_2 , indicating structural non-identifiability. Here we use a log-normal error model for the hydraulic head values with constant standard deviation σ . Observations then follow:

$$(3.9) \quad \log h_{\text{obs}} \sim \mathcal{N}(\log B_{\text{obs}} h(\theta), \sigma^2 I),$$

where $\theta = [T_1, T_2, R]^T$, and $h(\theta)$ is the fine-scale solution.

4. Results and Discussion. Here we present the results of our analysis of the three example models described in Section 3. The first example is simple but illustrates many of the key conceptual components of our approach, including both structural and practical non-identifiability; the second involves a differential equation in time that is solved numerically and utilises automatic differentiation to compute the Jacobian of the auxiliary mapping; and the third involves a differential equation in space that can be solved analytically but involves three parameters and structural non-identifiability. For this last example, we show how parameter non-identifiability and predictive uncertainty are related using the PWA approach.

4.1. Parameterised Normal Models. These examples are sufficiently simple that we can illustrate the core ideas analytically, and so we first outline some analytical results. We then present numerical results, produced without assuming these analytical results were available, using generic model-agnostic code.

We focus our analytical illustration on the Poisson limit model for simplicity, defined by (3.2). In this model, we expect only np to be identifiable, as the variance is equal to the mean. We will show that both symbolic (original parameters) and numerical (log-transformed parameters) approaches obtain this result.

We also present the results of numerical, likelihood-based analysis of both parameterised normal models. We consider the likelihood functions in both original parameterisation and our reparameterisations. Although the likelihood is invariant to reparameterisation, we see how the reparameterisation ‘brings out’ the separation of information concerning the identifiable and non-identifiable parameters.

4.1.1. Analytical results: Poisson limit model, original parameterisation. To first obtain the symbolic result we note, as above, that the auxiliary mapping in terms of untransformed parameters is given by

$$\phi(n, p) = \phi \left(\begin{bmatrix} n \\ p \end{bmatrix} \right) = \begin{bmatrix} np \\ np \end{bmatrix}.$$

The Jacobian of this mapping is given by

$$(4.1) \quad D\phi(n, p) = \begin{bmatrix} p & n \\ p & n \end{bmatrix}.$$

This is a function of n and p and clearly has a non-trivial null space for all n and p . As the Jacobian and the associated null space depend on (are given as a function of) n and p we refer to this as the ‘symbolic’ null space of the model. We can determine this by inspection, noting that vectors of the form

$$(4.2) \quad \alpha(n, p) = \begin{bmatrix} n \\ -p \end{bmatrix}$$

satisfy $D\phi(n, p)\alpha(n, p) = 0$ for all n and p . Thus the symbolic null space has dimension one and is spanned by the vector $\alpha(n, p)$; furthermore, the row space of $D\phi(n, p)$ hence has dimension one and is spanned by a symbolic vector orthogonal to $\alpha(n, p)$. This implies that $\psi(n, p)$ is scalar-valued and can be determined by equating the (unknown) single row of $D\psi(n, p)$ to the (transpose of the) vector spanning the (known) row space of $D\phi(n, p)$. By inspection, we see that the row space of $D\phi(n, p)$ is spanned by the vector $[p, n]^T$, which is orthogonal to $\alpha(n, p) = [n, -p]^T$.

Thus we can determine $\psi(n, p)$ equating the rows of $D\psi(n, p)$ to the vectors spanning the row space of $D\phi(n, p)$, or by solving the partial differential equation

$$(4.3) \quad \frac{\partial \psi}{\partial n} n + \frac{\partial \psi}{\partial p} (-p) = 0,$$

based on the orthogonality of the rows of $D\psi(n, p)$ and the vectors spanning the null space of $D\phi(n, p)$. By inspection, we see that $\psi(n, p) = np$ is a solution to these equations, and hence the identifiable parameterisation is given by $\psi(n, p) = np$, as expected. This approach is equivalent to that of [14, 29, 19, 18] but, as with their approach, requires symbolic determination of the Jacobian and the solution of partial differential equations. We now show how our numerical approach can determine the same result without symbolic manipulation.

4.1.2. Analytical results: Poisson limit model, log-transformed parameterisation. We now consider the Poisson limit model in log-transformed parameters. By definition (specifically, from parameterisation invariance) the auxiliary mapping in terms of log-transformed parameters satisfies

$$(4.4) \quad \phi_*(n^*, p^*) = \phi_* \left(\begin{bmatrix} n^* \\ p^* \end{bmatrix} \right) = \phi \left(\begin{bmatrix} n \\ p \end{bmatrix} \right) = \phi \left(\exp \left(\begin{bmatrix} n^* \\ p^* \end{bmatrix} \right) \right),$$

where $n^* = \log n$ and $p^* = \log p$ and where \exp is the componentwise exponential function.

The right-hand side of the above equation is obtained from the definition of the auxiliary mapping in terms of untransformed parameters:

$$(4.5) \quad \phi \left(\begin{bmatrix} n \\ p \end{bmatrix} \right) = \begin{bmatrix} np \\ np \end{bmatrix} = \begin{bmatrix} \exp(n^*) \exp(p^*) \\ \exp(n^*) \exp(p^*) \end{bmatrix} = \begin{bmatrix} \exp(n^* + p^*) \\ \exp(n^* + p^*) \end{bmatrix}$$

Thus the Jacobian of the auxiliary mapping in terms of log-transformed parameters is given by

$$(4.6) \quad D\phi_*(n^*, p^*) = \begin{bmatrix} \exp(n^* + p^*) & \exp(n^* + p^*) \\ \exp(n^* + p^*) & \exp(n^* + p^*) \end{bmatrix} = \exp(n^* + p^*) \begin{bmatrix} 1 & 1 \\ 1 & 1 \end{bmatrix}.$$

As expected, this takes the SVD form (up to normalisation of the singular vectors):

$$(4.7) \quad D\phi_*(n^*, p^*) = \underbrace{\begin{bmatrix} 1 \\ 1 \end{bmatrix}}_{D_{\psi_*} \tilde{\phi}(\psi_*(\theta^*))} \underbrace{\exp(n^* + p^*)}_{\text{diag}(\exp(A\theta^*))} \underbrace{\begin{bmatrix} 1 & 1 \end{bmatrix}}_A,$$

where $\theta^* = [n^*, p^*]^T$, A is the matrix of the constant linear transformation component of the reparameterisation and $D_{\psi_*} \tilde{\phi}(\psi_*(\theta^*))$ is the Jacobian of the auxiliary mapping in terms of the transformed, identifiable parameters. The diagonal ‘matrix’ is a scalar in this case as the intermediate image is represented by a single parameter. Since $\psi_*(n^*, p^*) = \exp(n^* + p^*)$, and the output of the auxiliary mapping is

$$(4.8) \quad \phi_*(n^*, p^*) = \begin{bmatrix} \exp(n^* + p^*) \\ \exp(n^* + p^*) \end{bmatrix} = \begin{bmatrix} \psi_*(n^*, p^*) \\ \psi_*(n^*, p^*) \end{bmatrix},$$

we have that $D_{\psi_*} \tilde{\phi}(\psi_*(\theta^*))$ is also constant in this case. In more general classes of models, the A matrix will remain constant, but the Jacobian of the auxiliary mapping in terms of the identifiable parameters will depend on the parameters.

Thus we conclude that the identifiable parameterisation is given by

$$(4.9) \quad \psi_*(n^*, p^*) = \exp(A\theta^*) = \exp \left(\begin{bmatrix} 1 & 1 \end{bmatrix} \begin{bmatrix} n^* \\ p^* \end{bmatrix} \right) = \exp(n^* + p^*) = \exp(\log n + \log p) = np.$$

This is the same result as obtained in the symbolic analysis above. However, as the A matrix here is constant, and corresponds (up to normalisation) to the singular vector of the Jacobian of the auxiliary mapping in log-transformed parameters, we can determine it with a single numerical evaluation of the Jacobian. This is the key advantage of our numerical approach.

We can also determine the non-identifiable parameters by considering the full SVD of the Jacobian (or by finding orthogonal vectors to the identifiable parameter combination). As before, this implies that the non-identifiable parameter combination is given by

$$(4.10) \quad \lambda_*(n^*, p^*) = \exp \left(\begin{bmatrix} 1 & -1 \end{bmatrix} \begin{bmatrix} n^* \\ p^* \end{bmatrix} \right) = \exp(n^* - p^*) = \frac{n}{p}.$$

4.1.3. Numerical results: Poisson limit model. Below we present the results of our numerical analysis of the Poisson limit model. We show the likelihood functions in both the original parameterisation and the ‘invariant image’ reparameterisation in Figure 3. We used true parameter values of $n = 100$ and $p = 0.2$, and a sample size of 10. We also imposed bounds of $[0, 500]$ and $[0, 1]$ for n and p , respectively. For reproducibility, the data realisation used was $[21.9, 22.3, 12.8, 16.4, 16.4, 20.3, 16.2, 20.0, 19.7, 24.4]$. This was generated from the *non-limit* model, i.e. treating the limit model as an approximation at the analysis rather than data generation stage. The analysis can be found in the [repository](#) at `examples/stat_model.jl`.

The top row of Figure 3 shows the likelihood in the original parameterisation,. We see a long ‘banana’ shaped likelihood contour in the (n, p) plane, illustrating the existence of (approximately) equivalent parameter combinations lying along a curved relationship. The profile likelihoods for each parameter illustrate the individual non-identifiability of the parameters. The likelihood is completely flat for both parameters, other than where the bounds of the parameter space are reached. Together these results imply that the two parameters are not individually identifiable in this model, though there may be some combination of parameters that is identifiable (i.e. np , as we have shown analytically).

The bottom row of Figure 3 shows the likelihood in reparameterised space. We see the likelihood is constant in the vertical, $\frac{n}{p}$, direction and varies only in the horizontal, np , direction. This reflects the identifiability of the parameter combination np , and the non-identifiability of the parameter combination n/p . Furthermore, this structure means the information concerning the identifiable and non-identifiable parameters is completely separated, as the likelihood factors into a product of a function of np and a (constant) function of n/p (see e.g. the discussion in [2, 22]). Thus we can, in principle, construct an autonomous reduced model based on the identifiable parameter combination np (as can be seen analytically).

The profile likelihoods for the new parameters, shown in the bottom row of Figure 3 further illustrate the distinct identifiability properties of these parameter combinations. The profile likelihood for np is a simple Gaussian-like function, showing good estimability, while the profile likelihood for n/p is completely flat, demonstrating non-identifiability.

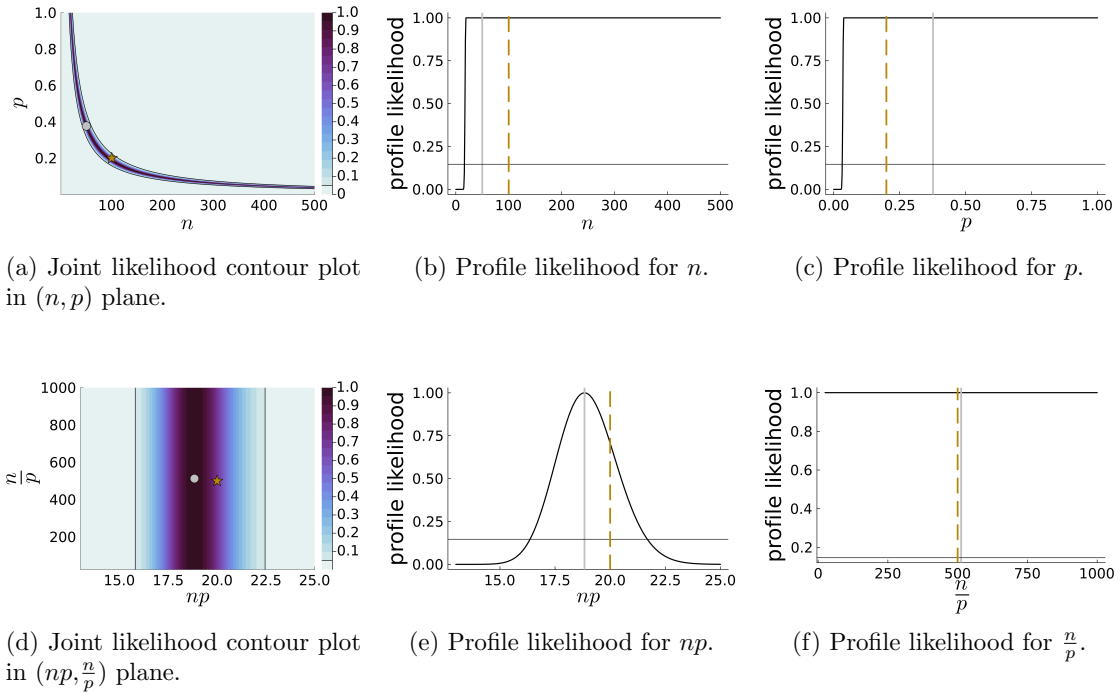


Figure 3: Poisson-limit example analysis in original (top row) and reparameterised (bottom row) parameter spaces. For the contour plots (left column), gold stars show the true parameter value, silver circles show the maximum likelihood estimate, and the colour bar represents the relative likelihood. For all plots, black contour/horizontal lines indicate the 95% confidence interval threshold. For profile likelihood plots (centre, right columns), the solid silver vertical line indicates the maximum likelihood estimate, and the dashed gold vertical line indicates the true parameter value.

4.1.4. Numerical results: non-limit model. We now consider the non-limit model, defined by (3.1). This model is now technically identifiable – for example, the mean and variance are now distinct as $np \neq np(1-p)$ for $p \neq 0$, and we can solve for n and p separately from these two quantities. However, near the Poisson limit, we also expect the parameters to be practically non-identifiable, i.e. poorly-identified. In this setting, the well-identified parameter determined from the SVD will be close but not exactly equal to np , while there will be a poorly identified parameter close to but not exactly equal to n/p . We can either work with the exact SVD singular vectors obtained, e.g., for our point estimate, or use the heuristic rounding approach to obtain the approximate reparameterisation. Here we find that our rounding heuristic (dividing by smallest non-zero entry and rounding to nearest 0.5) indeed recovers the previous identifiable and non-identifiable parameter combinations, but these now correspond to ‘well-identified’ and ‘poorly but structurally identified’ parameters, respectively.

For these results, again, we used true parameter values of $n = 100$ and $p = 0.2$, a sample

size of 10, and the same parameter bounds. For reproducibility, the data realisation used was (again) [21.9, 22.3, 12.8, 16.4, 16.4, 20.3, 16.2, 20.0, 19.7, 24.4]. The analysis can again be found in the [repository](#) at `examples/stat_model.jl`.

These results can be seen in Figure 4, and largely mirror those of the Poisson limit model. The well-identified parameter np and the poorly identified parameter n/p are again clearly separated in the reparameterised space. However, in this case, the separation is not exact, and the poorly identified parameter is not completely flat in the profile likelihood. We also see *one-sided identifiability* in both the original parameterisation and in the poorly identified parameter in the reparameterised model – the likelihood is much flatter on one side of the maximum likelihood estimate than the other. We can attribute this to the model becoming poorly identified in the Poisson limit, which occurs asymmetrically in parameter space.

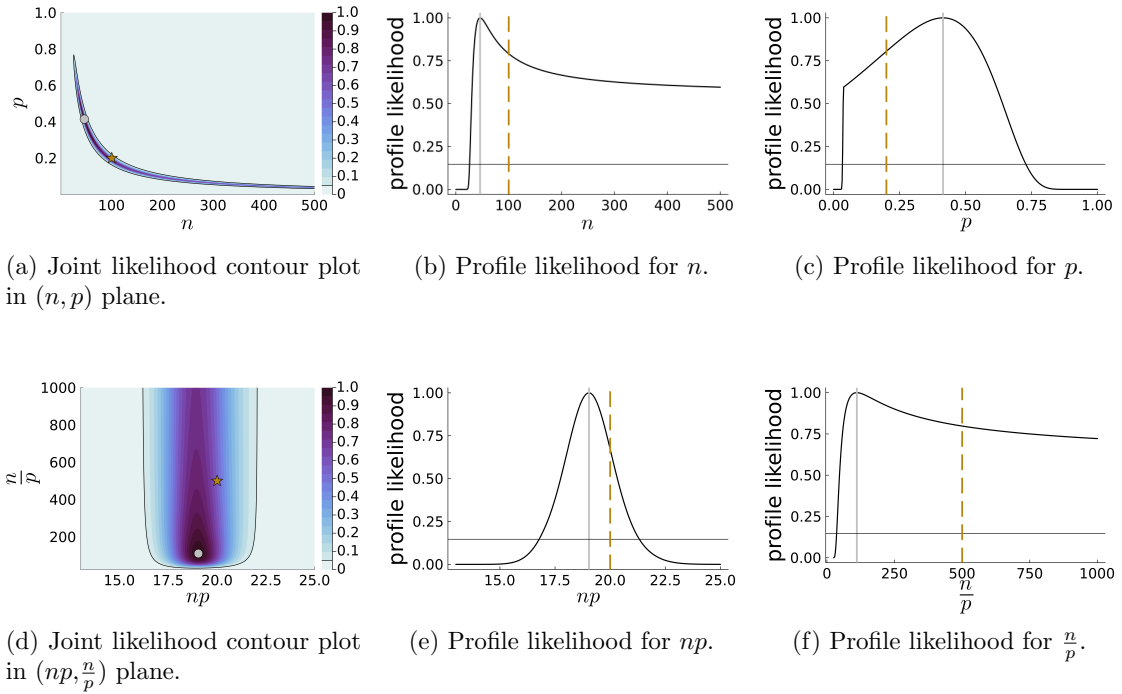


Figure 4: Non-limit (approximate Binomial) example analysis in original (top row) and reparameterised (bottom row) parameter spaces. For the contour plots (left column), gold stars show the true parameter value, silver circles show the maximum likelihood estimate, and the colour bar represents the relative likelihood. For all plots, black contour/horizontal lines indicate the 95% confidence interval threshold. For profile likelihood plots (centre, right columns), the solid silver vertical line indicates the maximum likelihood estimate, and the dashed gold vertical line indicates the true parameter value.

4.2. Michaelis-Menten kinetics. We now consider the Michaelis-Menten kinetics model, defined by (3.4). This model is structurally identifiable but practically non-identifiable in the limit regime where the initial substrate concentration, $S(0)$, is low relative to the half-saturation constant, K . For this example, we first focus on results from the non-reduced model before considering the reduced model. This reflects the more natural process of analysis, where identifiability analysis suggests the possibility of a reduced, structurally non-identified model, which could be investigated subsequently.

For these results, we used an initial concentration of $S(0) = 1$, a true half-saturation constant of $K = 5.0$, and a maximum growth rate of $\nu = 1.0$. We used a normal observation model with standard deviation $\sigma = 0.05$, and observed the concentrations at 11 equally spaced time points between 0 and 20. We used a fine time grid of 201 points between 0 and 20 for the model solution in the auxiliary mapping computations. This regime is relatively close to the limit regime, but not so close that the effects are negligible. We expect the parameters to be potentially practically non-identifiable in this regime, but structurally identifiable. Our analysis can be found in the [repository](#) at `examples/mm_model.jl`.

The top row of Figure 5 shows the results of the non-reduced model analysis in the original parameterisation. We see that the joint likelihood contours in the (ν, K) plane consist of ‘fanning’ lines, indicating the existence of parameter combinations having similar likelihood values. The profile likelihoods for each parameter show that the maximum likelihood estimate is close to the true parameter value in this particular case but that the likelihood is very flat to one side (excluding the effects of parameter bounds) and shows characteristic ‘one-sided identifiability’, i.e. limiting non-identifiability.

The bottom row of Figure 5 shows the results of the non-reduced model analysis in reparameterised space. Here the parameter combinations identified are $\frac{K}{\nu}$ (well-identified) and νK (poorly identified). The first parameter represents the time scale associated with the limit model. We see a similar likelihood contour shape to the previous model analysis, with an apparent limiting regime where the parameters are decoupled and one parameter is well-identified while the other is poorly identified. Outside of the limit regime, the relationship between the parameters is more complex, and the parameters are not as clearly separated. Since the likelihood is invariant to reparameterisation, analysis of the non-reduced model in any coordinate system is equally valid. The role of reparameterisation is to bring out the separation of information concerning the potentially identifiable and non-identifiable parameters.

Although only approximate, these results do suggest a structurally non-identified reduced model may be useful, in the limit as $K\nu$ becomes large while $\frac{K}{\nu}$ stays constant. This corresponds to the limit model mentioned in the model description section above.

Figure 6 shows the results of the limit (reduced) model analysis in the reparameterised space. We see the likelihood contours agree well in the limit regime, while keeping the separation of parameters in the non-limit regime where the approximation technically breaks down. The profile likelihoods show full non-identifiability of the poorly identified parameter, and good identifiability of the well-identified parameter. This is consistent with the expected behaviour of the reduced, structurally non-identifiable model.

For this model, we provide prediction results using PWA in the supplementary material and provide more detailed prediction results for the transport model next.

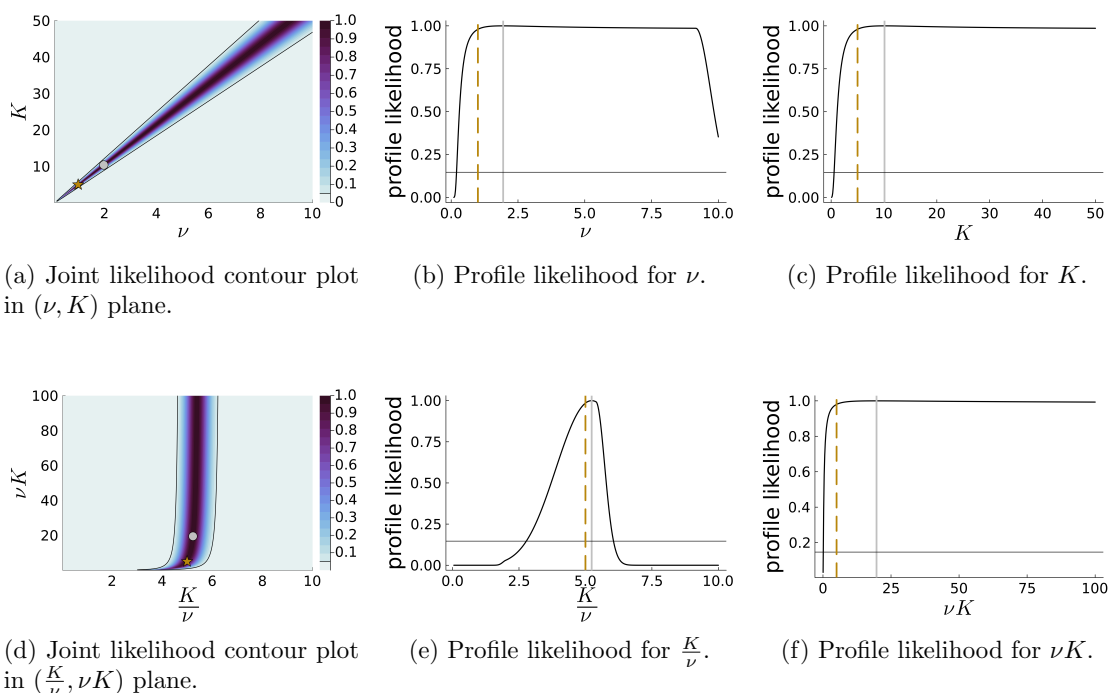


Figure 5: Michaelis-Menten example analysis in original (top row) and reparameterised (bottom row) parameter spaces. For the contour plots (left column), gold stars show the true parameter value, silver circles show the maximum likelihood estimate, and the colour bar represents the relative likelihood. For all plots, black contour/horizontal lines indicate the 95% confidence interval threshold. For profile likelihood plots (centre, right columns), the solid silver vertical line indicates the maximum likelihood estimate, and the dashed gold vertical line indicates the true parameter value.

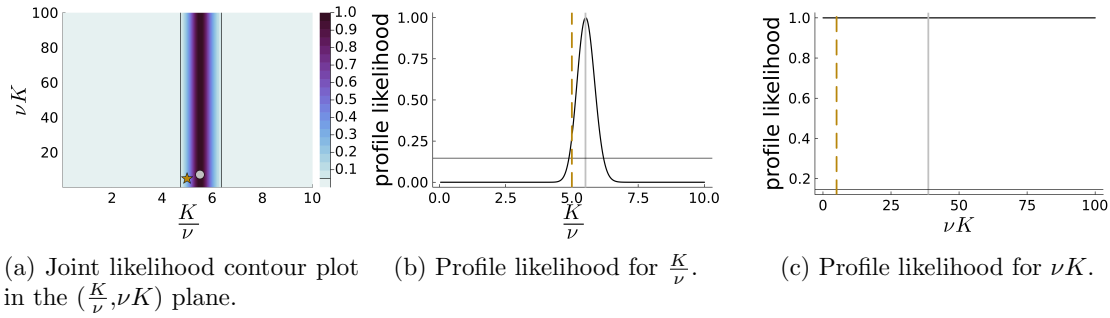


Figure 6: Reparameterised Michaelis-Menten limit example: (Left) joint contour in the $(\frac{K}{\nu}, \nu K)$ plane. The gold star indicates the true parameter value, and the silver circle indicates the maximum likelihood estimate. The colour bar represents the relative likelihood. (Centre and right) profile likelihoods. The solid silver vertical line indicates the maximum likelihood estimate, and the dashed gold vertical line indicates the true parameter value. For all plots, black contour/horizontal lines indicate the 95% confidence interval threshold.

4.3. Flow in heterogeneous media. Here we consider the groundwater model, representing flow in heterogeneous media, defined by (3.7). As discussed in the model section, and shown in the supplementary material, this model is structurally non-identifiable, and can be written in terms of a reduced set of monomial functions of the parameters. Rather than consider further analytical results, we proceed directly to the numerical analysis of the model and verify that our numerical approach can uncover the non-identifiability of the model and suggest a reduced parameterisation.

For these results we used a true parameter value of $T_1 = 3.0$, $T_2 = 1.0$, and $R = 1.0$, with parameter bounds of $[0.1, 5]$ for all quantities. We considered a fine grid of 201 points between $x = 0$ and $x = L = 100$, and an observation grid of 19 equally-spaced points, excluding the endpoints. We used a normal observation model with standard deviation $\sigma = 0.2$ and a single, spatial sample (i.e. a single observation of the model solution at the observation points, giving a data vector of length 19). For reproducibility, the data realisation used was [186.4, 402.6, 505.2, 756.1, 1144.1, 790.9, 1283.5, 1647.6, 872.3, 1144.4, 1691.2, 1352.7, 1519.9, 1316.0, 1437.1, 726.7, 952.3, 759.4, 272.0]. [repository](#) at `examples/transport_model.jl`.

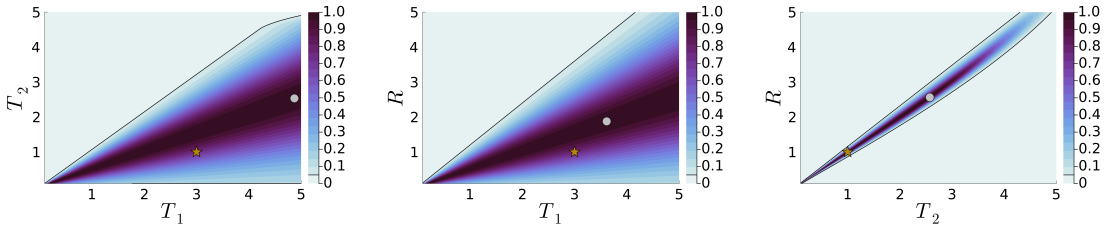
The first two rows of Figure 7 show the results of the analysis in the original parameterisation. For visualisation we consider each of the three joint two-dimensional likelihood profiles with the third parameter ‘profiled out’. We see that the joint profile likelihood contours in the (T_1, T_2) plane show a ‘fanning out’ of the likelihood contours, indicating the existence of parameter combinations having similar likelihood values. Similarly for (T_1, R) . For (T_2, R) we see more concentrated contours, indicating that some combination of these parameters may be better identified. We also show the one-dimensional profile likelihoods for each parameter. These all show largely flat likelihoods, other than decreases induced by bounding constraints, indicating that these parameters are not individually identifiable in this model.

The second two rows of Figure 7 show the analysis in the reparameterised space. The repara-

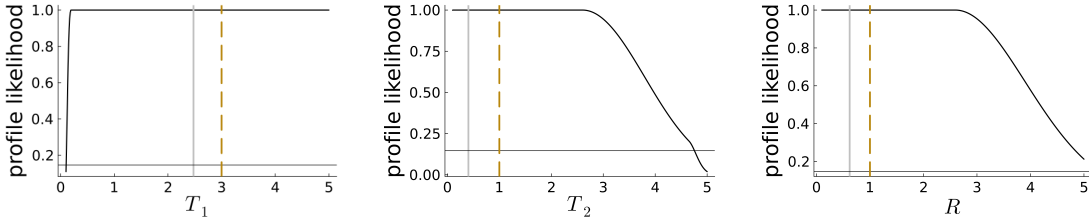
reparameterisation suggested by the SVD is $(\frac{T_2}{R}, \frac{T_1}{\sqrt{T_2 R}}, T_1 T_2 R)$, with the first having a singular value two-three orders of magnitude larger than the second, and the third being numerically equivalent to zero (order 10^{-14}). This indicates that one parameter combination is very well identified, the second somewhat identified, and the third completely unidentifiable. The first two combinations from the SVD reparameterisation are different to the reduced parameter pair that appear in the analytical results, i.e. to $(\frac{T_1}{R}, \frac{T_1}{R})$, though these are in one-to-one correspondence. This reflects that the SVD aims to find an orthogonal (in log-parameter space in the present work) reparameterisation in which the information on each parameter combination is maximally separated. Both pairs of parameter combinations are orthogonal to the non-identified parameter combination $T_1 T_2 R$ in log-space, and are linearly independent, and hence provide a valid basis for the identified subspace. Here the two parameterisations lead to visually indistinguishable results, and so we only show the results of the SVD reparameterisation.

Notably, the reparameterised results indicate possible one-sided identifiability of the less well (but still) identified parameter $\frac{T_1}{\sqrt{T_2 R}}$, in addition to the structural non-identifiability of $T_1 T_2 R$. This suggests a further reduced limiting model may exist. Here the true value of the first transmissivity parameter T_1 is somewhat larger than the second (three vs one), and the limit suggested by the one-sided non-identifiability is to take T_1 large relative to T_2 and R . Thus the smaller transmissivity parameter T_2 becomes the limiting factor in the model, and the model can be reduced to a simpler form. This reinforces that profile likelihood-based practical identifiability methods can help determine limiting models, as in [51] and as in the previous examples, though for this example we do not pursue this further.

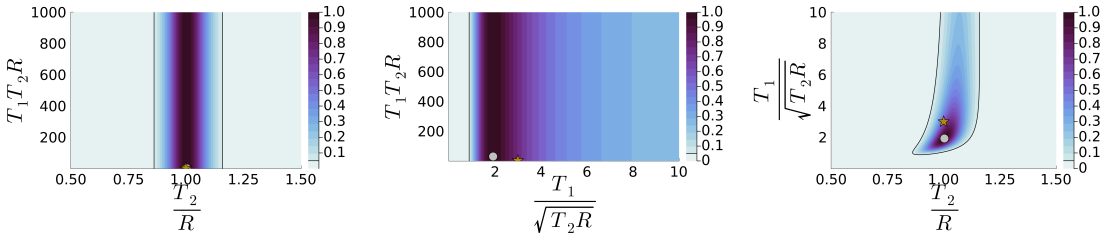
Finally, we show the profile-wise prediction intervals for the full model in the reparameterised space in Figure 8. We provide the profile-wise prediction intervals for the original parameterisation in the supplementary material. We use a degree of freedom of two for all of the prediction intervals (i.e. number of non-zero singular values and hence intrinsic dimensionality; see also [69]). In the original space the prediction intervals are driven by all three parameters (supplementary material). In the reparameterised space, however, we see that the non-identified parameter $T_1 T_2 R$ has no effect on the prediction intervals. This is true of both the individual profile-wise prediction interval based on $T_1 T_2 R$ in the bottom row, and the joint prediction intervals involving $T_1 T_2 R$ in the top row, which closely match the individual profile-wise prediction intervals for the other parameter in each case.



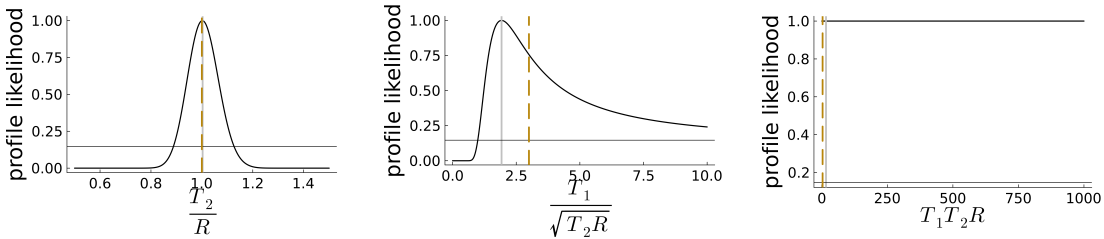
(a) Joint profile likelihood in (T_1, T_2) plane. (b) Joint profile likelihood in (T_1, R) plane. (c) Joint profile likelihood in (T_2, R) plane.



(d) Profile likelihood for T_1 . (e) Profile likelihood for T_2 . (f) Profile likelihood for R .



(g) Joint profile likelihood in $(\frac{T_2}{R}, \frac{T_1}{\sqrt{T_2R}})$ plane. (h) Joint profile likelihood in $(\frac{T_1}{\sqrt{T_2R}}, T_1T_2R)$ plane. (i) Joint profile likelihood in $(\frac{T_2}{R}, \frac{T_1}{\sqrt{T_2R}})$ plane.



(j) Profile likelihood for $\frac{T_2}{R}$. (k) Profile likelihood for $\frac{T_1}{\sqrt{T_2R}}$. (l) Profile likelihood for T_1T_2R .

Figure 7: Flow in heterogeneous media example analysis in original (top two rows) and reparameterised (bottom two rows) parameter spaces. First and third rows show joint likelihood contours; second and fourth rows show profile likelihoods. For contour plots, gold stars show the true parameter value, silver circles show the maximum likelihood estimate, and colorbars represent relative likelihood. For all plots, black contour/horizontal lines indicate the 95% confidence interval threshold. For profile likelihood plots, solid silver vertical lines show maximum likelihood estimates and dashed gold vertical lines show true parameter values.

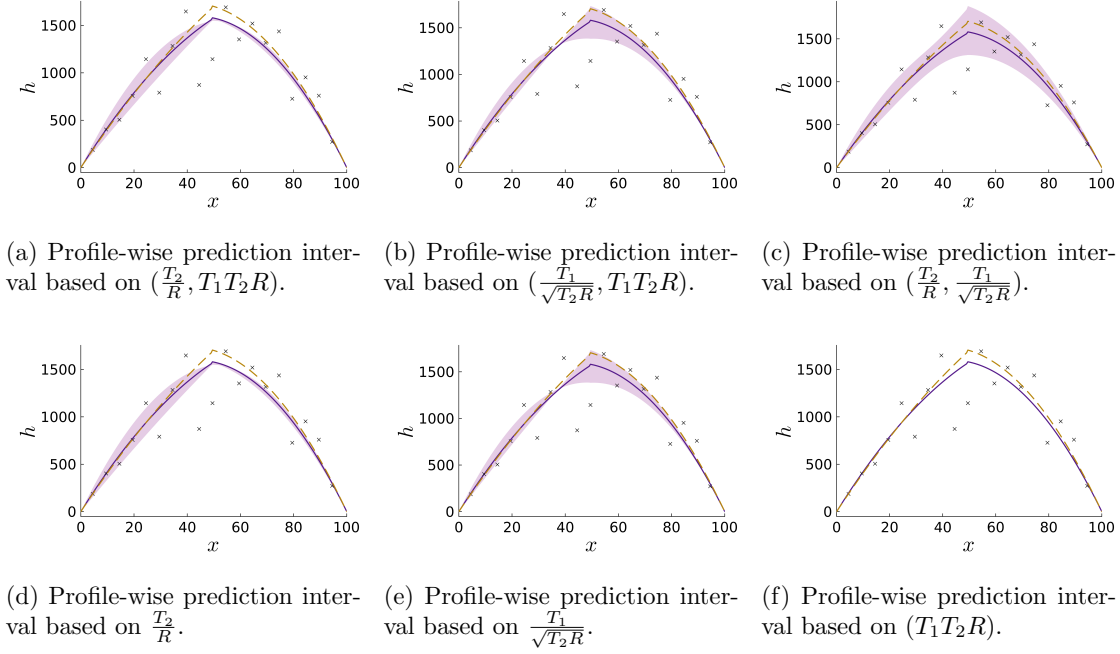


Figure 8: Profile-wise prediction intervals for the mean in the flow in heterogeneous media example in reparameterised space. Top row shows joint prediction intervals; bottom row shows individual parameter prediction intervals. In all plots, gold trajectories show the true mean function, dark purple trajectories show the maximum likelihood estimate, and purple shaded regions represent approximate 95% (predictive) confidence intervals for the mean.

5. Conclusions and Future Work. Here we have presented Invariant Image Reparameterisation (IIR), an approach to parameter identifiability analysis that bridges structural and practical identifiability analysis and symbolic and numerical methods of implementation. We show how an initial coordinate transformation can convert the symbolic approach of discovering identifiable parameter combinations into numerical computation at a single reference point. This numerical approach recovers symbolic results for a typical class of parameter combinations while providing a natural ranking of such parameter combinations by their degree of identifiability in general and in cases of practical non-identifiability. While IIR reduces reliance on symbolic methods, these remain useful in cases where the parameter combinations of interest are more complex than monomials and when the model is amenable to symbolic computation. Extending the present work to such cases is of interest for future work. Relatedly, it would be of interest to investigate the possibility of extending the parameter transformation approach of IIR to rational functions of parameters, as used for fitting to profile relationships in [27]. We emphasise, however, that monomial parameter combinations are common in practice based on dimensional considerations and asymptotic arguments connected to model reduction [3].

Relatedly, we find that practical non-identifiability, particularly when one-sided or asymmetric, is closely related to the existence of potential model reductions when a parameter combination becomes small or large, mirroring observations by [51] on using profile likelihood for model reduction. Our use of profile-likelihood-based Profile-Wise Analysis for uncertainty quantification, in addition to reparameterisation based on the auxiliary mapping (or Fisher information), reveals such asymmetric limits in terms of likelihood contours and profiles, in contrast to approaches focusing solely on Fisher-information/Hessian analysis.

As in [66], our framework in principle extends to more complex models such as stochastic differential equations or simulation-based models, given an appropriate auxiliary mapping. However, while here we used the full model solution as our ‘exhaustive summary’, stochastic or simulation-based models generally need more carefully defined data distribution parameters such as moment dynamics equations [10]. Additionally, while our approach applies in principle to larger models, we deliberately considered examples with low parameter dimension, as even these give complex results. Further work could explore applications to larger models and spatially/temporally varying parameters, as well as improving scaling and rounding heuristics for interpretable parameter combinations.

The provided **Julia implementation** makes our methodology accessible for future work and development. We believe IIR will prove valuable for modelling and data analysis across the quantitative sciences, particularly in complex applications where symbolic approaches may be impractical.

6. Acknowledgements. Parts of this work were carried out at the MATRIX Workshop on Parameter Identifiability in Mathematical Biology (2024) for which OJM and MJS were among the organisers. We thank MATRIX for funding this workshop and the participants for their stimulating discussions. MJS was supported by the Australian Research Council Centre of Excellence for Mathematical Analysis of Cellular Systems grant no. CE230100001 (MJS). Large Language Models (LLMs), including Claude (3.5 Sonnet by Anthropic) and ChatGPT (o1/o3-mini models by OpenAI), were used during manuscript refinement. These tools assisted with clarifying explanations, assessing technical arguments, suggesting ways to shorten the manuscript, and providing general editorial suggestions. Code refactoring for the accompanying Julia implementation was also aided by LLM suggestions (including Claude, ChatGPT, and GitHub Copilot). The article, including technical content, proofs, algorithm development, and analysis, was developed by the authors; the use of LLMs was solely for improving presentation and implementation. All LLM suggestions were critically evaluated before incorporation, and the authors take responsibility for their appropriate use in the final manuscript.

7. Author Contributions. All authors contributed to the review and editing of the manuscript. OJM wrote the original draft with contributions from MJS. Both OJM and MJS contributed to the conceptualisation of the article, choice of examples and design of numerical experiments. OJM developed the method details, proofs, wrote the code, and performed the numerical experiments, with discussion and input from the other authors.

8. Competing interests. The authors declare that they have no competing interests.

9. Data and materials availability. All data needed to evaluate the conclusions in the paper are present in the paper and/or the supplementary material. Julia code associated with this paper is available from GitHub at <https://github.com/omaclaren/reparam>.

REFERENCES

- [1] M. AITKIN, *Statistical inference: an integrated Bayesian/likelihood approach*, CRC Press, 2010.
- [2] M. AITKIN AND M. STASINOPOULOS, *Likelihood analysis of a binomial sample size problem*, Contributions to probability and statistics: Essays in honor of Ingram Olkin, (1989), pp. 496–499.
- [3] G. I. BARENBLATT, *Scaling*, Cambridge University Press, 2003.
- [4] J. BEAR, *Dynamics of fluids in porous media*, American Elsevier Publishing Company, 1972.
- [5] G. BELLU, M. P. SACCOMANI, S. AUDOLY, AND L. D’ANGIÓ, *DAISY: A new software tool to test global identifiability of biological and physiological systems*, Computer Methods and Programs in Biomedicine, 88 (2007), pp. 52–61.
- [6] R. BIRD, W. STEWART, AND E. LIGHTFOOT, *Transport phenomena*, no. v. 1 in Transport Phenomena, Wiley, 2006.
- [7] A. F. BROUWER AND M. C. EISENBERG, *The underlying connections between identifiability, active subspaces, and parameter space dimension reduction*, arXiv preprint arXiv:1802.05641, (2018).
- [8] K. S. BROWN, C. C. HILL, G. A. CALERO, C. R. MYERS, K. H. LEE, J. P. SETHNA, AND R. A. CERIONE, *The statistical mechanics of complex signaling networks: nerve growth factor signalling*, Physical Biology, 1 (2004), p. 184.
- [9] K. S. BROWN AND J. P. SETHNA, *Statistical mechanical approaches to models with many poorly known parameters*, Physical Review E, 68 (2003), p. 021904.
- [10] A. P. BROWNING, D. J. WARNE, K. BURRAGE, R. E. BAKER, AND M. J. SIMPSON, *Identifiability analysis for stochastic differential equation models in systems biology*, Journal of the Royal Society Interface, 17 (2020), p. 20200652.
- [11] E. BUCKINGHAM, *On physically similar systems; illustrations of the use of dimensional equations*, Physical review, 4 (1914), p. 345.
- [12] H. CARSLAW AND J. JAEGER, *Conduction of heat in solids*, Oxford science publications, Clarendon Press, 1959.
- [13] E. A. CATCHPOLE AND B. J. MORGAN, *Detecting parameter redundancy*, Biometrika, 84 (1997), pp. 187–196.
- [14] E. A. CATCHPOLE, B. J. T. MORGAN, AND S. N. FREEMAN, *Estimation in parameter-redundant models*, Biometrika, 85 (1998), pp. 462–468.
- [15] M. J. CHAPPELL AND R. N. GUNN, *A procedure for generating locally identifiable reparameterisations of unidentifiable non-linear systems by the similarity transform approach*, Mathematical Biosciences, 148 (1998), pp. 21–41.
- [16] O. CHIŞ, J. R. BANGA, AND E. BALSACANTO, *Structural identifiability of systems biology models: a critical comparison of methods*, Plos One, 6 (2011), p. e27755.
- [17] O. CHIŞ, A. F. VILLAVARDE, J. R. BANGA, AND E. BALSACANTO, *On the relationship between sloppiness and identifiability*, Mathematical Biosciences, 282 (2016), pp. 147–161.
- [18] D. COLE, *Parameter redundancy and identifiability*, CRC Press, 2020.
- [19] D. J. COLE, B. J. T. MORGAN, AND D. M. TITTERINGTON, *Determining the parameteric structure of models*, Mathematical Biosciences, 228 (2010), pp. 16–30.
- [20] P. G. CONSTANTINE, C. KENT, AND T. BUI-THANH, *Accelerating markov chain monte carlo with active subspaces*, SIAM Journal on Scientific Computing, 38 (2016), pp. A2779–A2805.
- [21] D. R. COX, *Principles of statistical inference*, Cambridge University Press, 2006.
- [22] D. R. COX AND N. REID, *Parameter orthogonality and approximate conditional inference*, Journal of the Royal Statistical Society: Series B (Methodological), 49 (1987), pp. 1–18.
- [23] J. CRANK, *The mathematics of diffusion*, Oxford university press, 1979.
- [24] T. CUI, J. MARTIN, Y. M. MARZOUK, A. SOLONEN, AND A. SPANTINI, *Likelihood-informed dimension reduction for nonlinear inverse problems*, Inverse Problems, 30 (2014), p. 1100998.

- [25] T. CUI AND X. TONG, *A unified performance analysis of likelihood-informed subspace methods*, Bernoulli, 28 (2022), pp. 2788–2815.
- [26] S. DÍAZ-SEOANE, X. REY BARREIRO, AND A. F. VILLAVARDE, *STRIKE-GOLDD 4.0: User-friendly, efficient analysis of structural identifiability and observability*, Bioinformatics, 39 (2022), p. btac748.
- [27] M. C. EISENBERG AND M. A. HAYASHI, *Determining identifiable parameter combinations using subset profiling*, Mathematical biosciences, 256 (2014), pp. 116–126.
- [28] C. R. ELEVITCH AND C. R. JOHNSON JR, *A procedure for ranking parameter importance for estimation in predictive mechanistic models*, Ecological Modelling, 419 (2020), p. 108948.
- [29] N. D. EVANS AND M. J. CHAPPELL, *Extensions to a procedure for generating locally identifiable reparameterisations of unidentifiable systems*, Mathematical Biosciences, 168 (2000), pp. 137–159.
- [30] C. R. FITTS, *Groundwater science*, Elsevier, 2002.
- [31] A. GELMAN, *Parameterization and bayesian modeling*, Journal of the American Statistical Association, 99 (2004), pp. 537–545.
- [32] A. GRIEWANK AND A. WALTHER, *Evaluating derivatives: principles and techniques of algorithmic differentiation*, SIAM, 2008.
- [33] R. N. GUTENKUNST, J. J. WATERFALL, F. P. CASEY, K. S. BROWN, C. R. MYERS, AND J. P. SETHNA, *Universally sloppy parameter sensitivities in systems biology models*, PLOS Computational Biology, 3 (2007), p. e189.
- [34] D. F. HENDRY AND M. S. MORGAN, *The foundations of econometric analysis*, Cambridge University Press, 1997.
- [35] K. E. HINES, T. R. MIDDENDORF, AND R. W. ALDRICH, *Determination of parameter identifiability in nonlinear biophysical models: A Bayesian approach*, Journal of General Physiology, 143 (2014), p. 401.
- [36] A. HOLMBERG, *On the practical identifiability of microbial growth models incorporating michaelis-menten type nonlinearities*, Mathematical Biosciences, 62 (1982), pp. 23–43.
- [37] F. HORN AND R. JACKSON, *General mass action kinetics*, Archive for Rational Mechanics and Analysis, 47 (1972), pp. 81–116.
- [38] P. HOWELL, G. KOZYREFF, AND J. OCKENDON, *Applied Solid Mechanics*, Cambridge University Press, 2008.
- [39] K. A. JOHNSON AND R. S. GOODY, *The original michaelis constant: Translation of the 1913 michaelis-menten paper*, Biochemistry, 50 (2011), pp. 8264–8269.
- [40] M. KOT, *Elements of Mathematical Ecology*, Cambridge University Press, 2001.
- [41] W. B. KRANTZ, *Scaling Analysis in Modeling Transport and Reaction Processes*, Wiley Interscience, 2007.
- [42] C. KREUTZ, A. RAUE, D. KASCHEK, AND J. TIMMER, *Profile likelihood in systems biology*, The FEBS Journal, 280 (2013), pp. 2564–2571.
- [43] C. KREUTZ, A. RAUE, AND J. TIMMER, *Likelihood-based observability analysis and confidence intervals for predictions of dynamics models*, BMC Systems Biology, 6 (2012).
- [44] J. LAWRIE AND J. HEARNE, *Reducing model complexity via output sensitivity*, Ecological Modelling, 207 (2007), pp. 137–144.
- [45] F. W. LAWVERE AND R. ROSEBRUGH, *Sets for mathematics*, Cambridge University Press, 2003.
- [46] J. LEE, *Introduction to smooth manifolds*, Graduate Texts in Mathematics, Springer New York, 2013.
- [47] T. S. LIGON, F. FRÖLICH, O. CHIŞ, J. R. BANGA, E. BALSACANTO, AND J. HASENAUER, *Genssi 2.0: multi-experimental structural identifiability analysis of sbml models*, Bioinformatics, 34 (2018), pp. 1421–1423.
- [48] O. J. MACLAREN AND R. NICHOLSON, *What can be estimated? identifiability, estimability, causal inference and ill-posed inverse problems*, arxiv preprint, 1904.02826 (2019).
- [49] O. J. MACLAREN AND R. NICHOLSON, *Models, identifiability, and estimability in causal inference*, in Workshop on the Neglected Assumptions in Causal Inference (NACI) at the 38th International Conference on Machine Learning, 2021, 2021.
- [50] J. R. MAGNUS AND H. NEUDECKER, *Matrix differential calculus with applications in statistics and econometrics*, John Wiley & Sons, 2019.
- [51] T. MAIWALD, H. HASS, B. STEIERT, J. VANLIER, R. ENGESSER, A. RAUE, F. KIPKEEW, H. H. BOCK, D. KASCHEK, C. KREUTZ, AND J. TIMMER, *Driving the model to its limit: Profile likelihood based model reduction*, Plos One, 11 (2016), p. e0162366.

- [52] N. MESHKAT, M. EISENBERG, AND J. J. DiSTEFANO III, *An algorithm for finding globally identifiable parameter combinations of nonlinear ode models using Gröbner bases*, *Mathematical Biosciences*, 222 (2009), pp. 61–72.
- [53] N. MESHKAT, S. SULLIVANT, AND M. EISENBERG, *Identifiability results for several classes of linear compartment models*, *Bulletin of Mathematical Biology*, 77 (2015), p. 1620–1651.
- [54] J. MONOD, *The growth of bacterial cultures*, *Annual Review of Microbiology*, 3 (1949), pp. 371–394.
- [55] G. M. MONSALVE-BRAVO, B. A. J. LAWSON, C. DROVANDI, K. BURRAGE, K. S. BROWN, C. M. BAKER, S. A. VOLLERT, K. MENGERSEN, E. McDONALD-MADDEN, AND M. P. ADAMS, *Analysis of sloppiness in model simulations: unveiling parameter uncertainty when mathematical models are fitted to data*, *Science Advances*, 8 (2022), p. eabm5952.
- [56] G. M. MONSALVE-BRAVO, B. A. J. LAWSON, C. DROVANDI, K. BURRAGE, K. S. BROWN, C. M. BAKER, S. A. VOLLERT, K. MENGERSEN, E. McDONALD-MADDEN, AND M. P. ADAMS, *Analysis of sloppiness in model simulations: Unveiling parameter uncertainty when mathematical models are fitted to data*, *Science Advances*, 8 (2022).
- [57] R. J. MURPHY, O. J. MACLAREN, AND M. J. SIMPSON, *Implementing measurement error models with mechanistic mathematical models in a likelihood-based framework for estimation, identifiability analysis and prediction in the life sciences*, *Journal of the Royal Society Interface*, 21 (2024), p. 20230402.
- [58] J. MURRAY, *Mathematical biology I: An introduction*, Springer, 2002.
- [59] I. OLKIN, A. J. PETKAU, AND J. V. ZIDEK, *A comparison of n estimators for the binomial distribution*, *Journal of the American Statistical Association*, 76 (1981), pp. 637–642.
- [60] L. PACE AND A. SALVAN, *Principles of statistical inference from a neo-Fisherian perspective*, World Scientific, 1997.
- [61] Y. PAWITAN, *In all likelihood: statistical modelling and inference using likelihood*, Oxford University Press, 2001.
- [62] A. RAUE, J. KARLSSON, M. P. SACCOMANI, M. JIRSTRAND, AND J. TIMMER, *Structural and practical identifiability analysis of partially observed dynamical models by exploiting the profile likelihood*, *Bioinformatics*, 30 (2014), pp. 1440–1448.
- [63] J. REVELS, M. LUBIN, AND T. PAPAMARKOU, *Forward-mode automatic differentiation in Julia*, arXiv preprint arXiv:1607.07892, (2016).
- [64] K. R. RUSHTON, *Groundwater hydrology: conceptual and computational models*, John Wiley & Sons, 2004.
- [65] M. J. SIMPSON, R. E. BAKER, S. T. VITTADELLO, AND O. J. MACLAREN, *Parameter identifiability analysis for spatiotemporal models of cell invasion*, *Journal of the Royal Society Interface*, 17 (2020).
- [66] M. J. SIMPSON AND O. J. MACLAREN, *Profile-wise analysis: A profile likelihood-based workflow for identifiability analysis, estimation, and prediction with mechanistic mathematical models*, *PLOS Computational Biology*, 19 (2023), p. e1011515.
- [67] M. J. SIMPSON AND O. J. MACLAREN, *Making predictions from nonidentifiable models.*, *Bulletin of Mathematical Biology*, 86 (2024), p. 80.
- [68] G. STEWART, *Matrix perturbation theory*, Computer Science and Scientific Computing/Academic Press, Inc, (1990).
- [69] J. TRENT, *Likelihood-based computational analysis and uncertainty quantification for mechanistic models*, master’s thesis, University of Auckland, 2024.
- [70] A. F. VILLAVERDE, E. RAIMÚNDEZ, J. HASENAUER, AND J. R. BANGA, *Assessment of prediction uncertainty quantification methods in systems biology*, *IEEE/ACM Transactions on Computational Biology and Bioinformatics*, 30 (2023), pp. 1725–1736.
- [71] S. A. VOLLERT, C. DROVANDI, G. M. MONSALVE-BRAVO, AND M. P. ADAMS, *Strategic model reduction by analysing model sloppiness: A case study in coral calcification*, *Environmental Modelling & Software*, 159 (2023), p. 105578.
- [72] F.-G. WIELAND, A. L. HAUBER, M. ROSENBLATT, T. C. AND J. TIMMER, *On structural and practical identifiability.*, *Current Opinion in Systems Biology*, 25 (2021).

SUPPLEMENTARY MATERIALS: Invariant Image Reparameterisation: A Unified Approach to Structural and Practical Identifiability and Model Reduction

Oliver J. Maclaren*, Ruanui Nicholson*, Joel A. Trent*, Joshua Rottenberry†, and Matthew J. Simpson‡

SM1. Mathematical theory and proofs. Here, we sketch some additional mathematical details and justifications omitted from the main text.

SM1.1. Null space/kernel properties. We frequently make use of the fact that if a matrix A is injective, i.e. has linearly independent columns, then, for any compatible matrices B, C , the relationship

$$(SM1.1) \quad AB = C$$

implies that

$$(SM1.2) \quad \ker B = \ker C.$$

This is an elementary result from linear algebra, but we provide a proof for completeness.

Proof. Suppose $x \in \ker B$. Then $Bx = 0$, and so $ABx = Cx = 0$. Thus $x \in \ker C$. Conversely, suppose $x \in \ker C$. Then $Cx = 0$, and so $ABx = Cx = 0$. Since A has linearly independent columns it is left invertible with pseudo-inverse A^+ , and so $A^+ABx = Bx = A^+0 = 0$ and $x \in \ker B$. Thus $\ker B = \ker C$. ■

This result naturally extends to the case of multiple injective matrices, e.g., $A_1A_2B = C$ implies $\ker B = \ker C$ for injective A_1 and A_2 . This is used in the parameter space linearisation section, where we also use the elementary fact that a diagonal matrix is injective if and only if all its diagonal entries are non-zero, which is true for a diagonal matrix with exponential function entries as considered in the main text.

SM1.2. Fisher information analysis. As mentioned in the main text, we can equivalently work with either the auxiliary mapping or observed Fisher information on the same grid level. Here we assume this is the solution grid level. We can also work with the finite data observed Fisher information, but this will not generally exactly recover the structural identifiability results due to additional discretisation. We can also work with the expected Fisher information, but prefer to consider the observed Fisher information as it is more directly related to the bridge between practical identifiability and structural identifiability. The link between identification and expected Fisher information for exponential family models discussed in [SM3]. An early reference for this link between identification and expected Fisher information for exponential family models is [SM2].

*Department of Engineering Science and Biomedical Engineering, University of Auckland, Auckland 1142, New Zealand.

†School of Mathematical Sciences, Queensland University of Technology (QUT), Brisbane, Australia.

‡ARC Centre of Excellence for the Mathematical Analysis of Cellular Systems, QUT, Brisbane, Australia.

To obtain the required result for the observed Fisher information, we first consider the transformation of the observed Fisher information under a change of parameters. Given the observed Fisher information in terms of the data distribution parameters, ϕ , and the Jacobian of the auxiliary mapping, $\phi_\theta(\theta)$, using subscripts to denote derivatives, we can write the observed Fisher information in terms of the mechanistic model parameters, θ , as

$$(SM1.3) \quad \begin{aligned} \mathcal{J}(\theta) &= \phi_\theta(\theta)^T l_{\phi\phi}(\phi(\theta); y) \phi_\theta(\theta) + (l_\phi(\phi(\theta); y) \otimes I_m) \phi_{\theta\theta}(\theta) \\ &= \phi_\theta(\theta)^T \mathcal{J}(\phi(\theta)) \phi_\theta(\theta) + (l_\phi(\phi(\theta); y) \otimes I_m) \phi_{\theta\theta}(\theta), \end{aligned}$$

where \otimes is the Kronecker matrix product, and where the above follows from the chain rule for matrix derivatives [SM4]; see also [SM1, SM5].

Now, we assume that, as a function of the data distribution parameters, ϕ , with fixed data y , the log-likelihood $l(\phi; y)$ has a solution $\hat{\phi}$ to the first-order score equations $l_\phi(\phi; y) = 0$ in the mechanistically parameterised range, $\phi[\Theta]$. We generally assume this occurs in the interior of this range, but allow for the possibility that this is approximately satisfied at or near a boundary. We then call any mechanistic model parameter θ for which $\phi(\theta) = \hat{\phi}$ a maximum likelihood (technically, zero score) estimate of θ and denote it by $\hat{\theta}$. This enables us to drop the second term in the above expression, giving the following transformation law for the observed Fisher information:

$$(SM1.4) \quad \mathcal{J}(\hat{\theta}) = \phi_\theta(\hat{\theta})^T \mathcal{J}(\hat{\phi}) \phi_\theta(\hat{\theta}).$$

This transformation law of the observed Fisher information evaluated at the maximum likelihood is a well-known result when $\phi(\theta)$ defines a one-to-one reparameterisation [SM5, SM1] but, as shown, continues to hold even when ϕ is not one-to-one (as long as, essentially, the true data distribution can be obtained by some mechanistic model, i.e. $\phi_{\text{true}} \in \phi[\Theta]$).

Next, we assume the observed Fisher information, $\mathcal{J}(\phi)$, as considered in terms of data distribution parameters rather than ‘mechanistic’ model parameters, is non-singular. Hence it is positive definite and we have $\mathcal{J}(\phi) = L^T L$ for some invertible square matrix L , and so

$$\begin{aligned} \mathcal{J}(\hat{\theta}) &= \phi_\theta(\hat{\theta})^T \mathcal{J}(\hat{\phi}) \phi_\theta(\hat{\theta}) \\ &= \phi_\theta(\hat{\theta})^T L^T L \phi_\theta(\hat{\theta}) \\ &= (L \phi_\theta(\hat{\theta}))^T (L \phi_\theta(\hat{\theta})). \end{aligned}$$

Since $\text{rank}(A^T A) = \text{rank}(A)$ for any matrix A , and $\text{rank}(BC) = \text{rank}(C)$ when B is invertible, it follows directly that

$$\text{rank}(\mathcal{J}(\hat{\theta})) = \text{rank}(\phi_\theta(\hat{\theta})).$$

The same essential result is given by [SM2] in the context of the expected Fisher information and exponential family models.

In the case of spatial or temporal data, the data distribution parameters (exhaustive summaries) will generally be given by the solution at the fine grid level. If the Fisher information is only defined at the observation grid level then we would need to use $\phi_{\text{obs}} = B_{\text{obs}} \phi$ instead of ϕ in the above. If B_{obs} has a nontrivial null space, $\text{rank}(\mathcal{J}(\hat{\theta}))$ will inherit this as well and certain parameter effects become unobservable at the discretisation level. This implies that

some parameters that are structurally identifiable at the fine grid level may appear practically non-identifiable at the observation grid level. Hence equivalence between the auxiliary mapping and observed Fisher information formulations requires a consistent choice of grid level.

SM2. Additional analytical results: flow in heterogeneous media. Here, we provide the analytical solution for the flow in heterogeneous media model considered in the main text. This model can be integrated twice in each region, then matched at the interface to give a piecewise quadratic solution. The solution is given by the solution to this equation is piecewise quadratic, given by

$$(SM2.1) \quad h(x) = \begin{cases} -\frac{1}{2} \left(\frac{R}{T_1} \right) x^2 + \alpha_1 x + \beta_1, & x < \frac{L}{2} \\ -\frac{1}{2} \left(\frac{R}{T_2} \right) x^2 + \alpha_2 x + \beta_2, & x \geq \frac{L}{2} \end{cases}$$

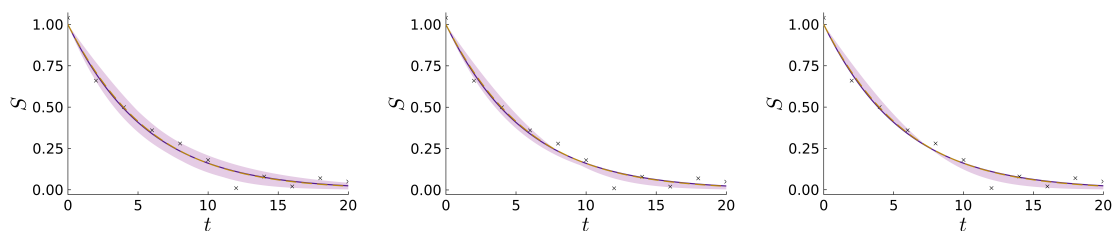
where α_i and β_i are constants determined by the boundary and interface conditions. From $h(0) = 0$ we have $\beta_1 = 0$, and from the flux continuity condition at $x = L/2$ we find $\alpha_1 = \alpha_2 = \alpha$. The remaining conditions, $h(L) = 0$ and continuity of h at $x = L/2$, give

$$(SM2.2) \quad \begin{aligned} \alpha &= \frac{3L}{8} \left(\frac{R}{T_2} \right) + \frac{L}{8} \left(\frac{R}{T_1} \right), \\ \beta_2 &= \frac{L^2}{8} \left[\left(\frac{R}{T_2} \right) - \left(\frac{R}{T_1} \right) \right]. \end{aligned}$$

As can be seen, the solution only depends on two ratios of the three parameters: R/T_1 and R/T_2 .

SM3. Additional results. Here, we provide some additional numerical results for the Michaelis-Menten and heterogeneous media flow models.

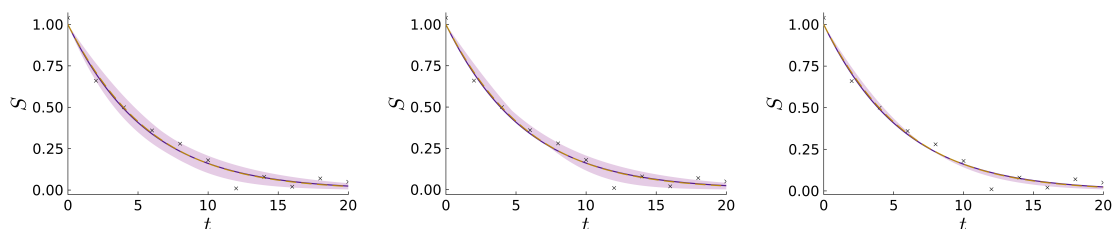
SM3.1. Michaelis-Menten model results. Here, we show the prediction results for the non-reduced model. For both the original and reparameterised model we show both the profile-wise prediction intervals [SM6] capturing the uncertainty in the prediction driven approximately solely by the target parameter, and the joint prediction intervals, capturing the uncertainty in the prediction due to both parameters. For both profile-wise and joint prediction intervals we use the 95% confidence level at 2 degrees of freedom in order to compare the ability of individual parameters to capture the joint uncertainty. The choice of degrees of freedom for prediction is investigated in more detail in [SM7]. These results are shown in Figure SM1. We see that in the reparameterised model the profile-wise prediction interval driven by the *well-identified* parameter captures more of the uncertainty in the prediction, while the poorly identified parameter has less effect, while in the original model both parameters contribute more equally to the prediction uncertainty. This effect becomes more pronounced the more non-identified the poorly-identified parameter becomes (see, e.g., the heterogeneous media flow example). Thus the reparameterised model supports model reduction in the predictive sense as well, at least approximately. Importantly, however, this is ‘within sample’ prediction, and the uncertainty in genuinely new domains may depend more strongly on the poorly identified parameter.



(a) Joint prediction interval based on (ν, K) parameterisation.

(b) Profile-wise prediction interval based on ν .

(c) Profile-wise prediction interval based on K .



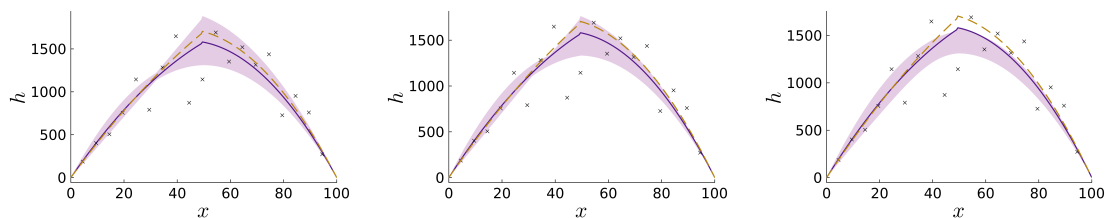
(d) Joint prediction interval based on $(\frac{K}{\nu}, \nu K)$ parameterisation.

(e) Profile-wise prediction interval based on $\frac{K}{\nu}$.

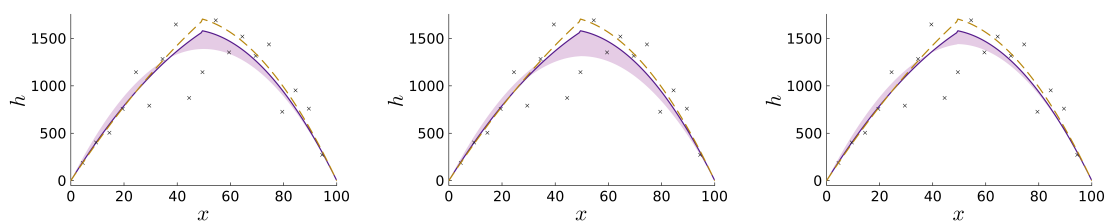
(f) Profile-wise prediction interval based on νK .

Figure SM1: Predictive confidence intervals for the mean in the Michaelis-Menten example in original (top row) and reparameterised (bottom row) parameter spaces. For all plots, the gold trajectory shows the true mean function, and the dark purple trajectory shows the maximum likelihood estimate. Purple shaded regions represent approximate 95% (predictive) confidence intervals for the mean. Left column shows joint prediction intervals; center and right columns show profile-wise prediction intervals for individual parameters.

SM3.2. Flow model results. Here, we show profile-wise prediction intervals for the original parameterisation of the flow in heterogeneous media model. As can be seen in Figure SM2, in the original space the prediction intervals are driven by all three parameters. This contrasts with the reparameterised space, where the prediction intervals are driven by only two of the three parameters (main text).



(a) Profile-wise prediction interval based on (T_1, T_2) . (b) Profile-wise prediction interval based on (T_1, R) . (c) Profile-wise prediction interval based on (T_2, R) .



(d) Profile-wise prediction interval based on T_1 . (e) Profile-wise prediction interval based on T_2 . (f) Profile-wise prediction interval based on R .

Figure SM2: Profile-wise prediction intervals for the mean in the flow in heterogeneous media example in original parameter spaces. Top row shows joint prediction intervals; bottom row shows individual parameter prediction intervals. In all plots, gold trajectories show the true mean function, dark purple trajectories show the maximum likelihood estimate, and purple shaded regions represent approximate 95% (predictive) confidence intervals for the mean.

REFERENCES

- [1] O. BARNDORFF-NIELSEN, *Information and exponential families: in statistical theory*, John Wiley & Sons, 2014.
- [2] E. A. CATCHPOLE AND B. J. MORGAN, *Detecting parameter redundancy*, *Biometrika*, 84 (1997), pp. 187–196.
- [3] D. COLE, *Parameter redundancy and identifiability*, CRC Press, 2020.
- [4] J. R. MAGNUS AND H. NEUDECKER, *Matrix differential calculus with applications in statistics and econometrics*, John Wiley & Sons, 2019.
- [5] L. PACE AND A. SALVAN, *Principles of statistical inference from a neo-Fisherian perspective*, World Scientific, 1997.
- [6] M. J. SIMPSON AND O. J. MACLAREN, *Profile-wise analysis: A profile likelihood-based workflow for identifiability analysis, estimation, and prediction with mechanistic mathematical models*, *PLOS Computational Biology*, 19 (2023), p. e1011515.
- [7] J. TRENT, *Likelihood-based computational analysis and uncertainty quantification for mechanistic models*, master's thesis, University of Auckland, 2024.